RSC Advances

PAPER

View Article Online
View Journal | View Issue

Cite this: *RSC Adv.*, 2017, **7**, 8688

Construction of a well-dispersed Ag/graphene-like g-C_3N_4 photocatalyst and enhanced visible light photocatalytic activity†

Hao Li,[a] Yue Jing,[a] Xinlong Ma,[a] Tongyao Liu,[a] Linfeng Yang,[a] Bin Liu,[a] Shu Yin,[b] Yongzhi Wei[a] and Yuhua Wang*[a]

Received 8th November 2016
Accepted 22nd January 2017

DOI: 10.1039/c6ra26498k

rsc.li/rsc-advances

In order to overcome the intrinsic drawback of pristine g-C_3N_4, we demonstrate a simple thermal oxidation exfoliation-photodeposition technique to fabricate a Ag/graphene-like g-C_3N_4 (Ag/G-g-C_3N_4) photocatalyst. It was revealed that the monodispersed Ag nanoparticles were well dispersed on the surface of graphene-like g-C_3N_4 (G-g-C_3N_4). The Ag/G-g-C_3N_4 displayed an enhanced photocatalytic activity for methylene blue degradation and the degradation rate was 10 times higher than that of pristine g-C_3N_4 under visible light irradiation. The enhancement of photocatalytic activity could be attributed to the surface plasmon resonance effect of Ag and large surface area (189.9 m^2 g^{-1}) of G-g-C_3N_4, which improve the visible light absorption ability and provide abundant reactive sites as well as promoting photogenerated electron–hole pair separation.

Introduction

In the course of the development of economy, some issues on environmental pollution emerged, which have restricted the sustainable development of modern human society.[1,2] The semiconductor photocatalytic technique, using renewable solar energy to degrade organic pollutants to non-toxic products, has been of interest to many researchers.[3,4] To date, many kinds of semiconductors have been explored for photocatalytic air purification and waste water treatment. They are mainly inorganic semiconductors, such as TiO_2, ZnO and Ag_3PO_4.[5–7] Nevertheless, materials with efficient activity and adequate stability for the degradation of pollutants under visible light irradiation are still unavailable, and their development remains a significant challenge.[8]

In recent years, a novel metal-free polymer semiconductor, g-C_3N_4 with a band gap of about 2.7 eV, has showed promising performance for hydrogen production and pollutant degradation under visible light irradiation.[9] Compared with their inorganic semiconductor counterparts, g-C_3N_4 is a sustainable and environmentally friendly organic semiconductor that consists of carbon and nitrogen, which are among the most abundant elements on our planet.[10] It has been clearly demonstrated that the metal-free π-conjugated g-C_3N_4 photocatalyst possesses interesting electronic properties as well as high thermal and chemical stability, therefore making them valuable materials for photocatalytically driven hydrogen production and pollutants degradation.[11]

However, there are still some key problems that restricted the application of g-C_3N_4 in environmental remediation,[12] such as, the low surface area and high recombination rate of photogenerated electron–hole pairs.[3,13] To solve these problems, many strategies such as introducing heteroatoms[14] or nitrogen vacancy,[15] coupling with other semiconductors or noble metal nanoparticles (Au, Ag),[16–18] controlling morphology[19] have been employed, and these g-C_3N_4-based photocatalysts have shown encouraging activity improvement.

Among various methods, construction of metal–semiconductor composites with surface plasmon resonance effect is a promising method. Moreover, the morphology control of g-C_3N_4 will intensively increase the photocatalytic activity.

Recently, Niu *et al.* developed a simple method to prepare graphene-like g-C_3N_4 (G-g-C_3N_4) by direct thermal oxidation process of bulk g-C_3N_4 in air.[20] The nanosheets possess not only a large surface area and small sheet thickness but also a short bulk diffusion length for reducing the recombination probability of photoexcited charge carriers. Whereas, the larger bandgap of resultant nanosheets hinders its visible light absorption capacity. Furthermore, Ge *et al.* prepared Ag/g-C_3N_4 composite photocatalysts *via* a heating method.[21] Bu *et al.* reported that Ag nanoparticles modified onto the g-C_3N_4 surface through photo-assisted reduction and studied the degradation performance for Rhodamine B.[22] The photocatalytic performance of g-C_3N_4 can be improved with the existence of Ag

[a]*Department of Materials Science, School of Physical Science and Technology, Lanzhou University, Lanzhou, 730000, China. E-mail: wyh@lzu.edu.cn; Fax: +86-931-8913554; Tel: +86-931-8912772*

[b]*Institute of Multidisciplinary Research for Advanced Materials, Tohoku University, 2-1-1 Katahira, Aoba-ku, Sendai, Japan*

† Electronic supplementary information (ESI) available. See DOI: 10.1039/c6ra26498k

nanoparticles. However, g-C_3N_4 in the Ag/g-C_3N_4 composite shows graphitic structure (low surface area), and Ag nanoparticles cannot well dispersed on the surface of g-C_3N_4. In a word, the previous studies did not reflect the advantage of the synergic effect between the surface plasmon resonance effect and the controlling of morphology. So the enhancement of photocatalytic activity in these works was not obvious.

Herein, inspired by above analyses, we designed Ag/graphene-like g-C_3N_4 (Ag/G-g-C_3N_4) photocatalyst by a simple method. The synthesized sample possesses not only the surface plasmon resonance effect of Ag but also a large surface area, which shows an enhanced photocatalytic activity.

Experimental

Synthesis of the pristine g-C_3N_4 and G-g-C_3N_4

The pristine g-C_3N_4 powder was synthesized by one-step polymerization of 5 g melamine according to the literature.[9] In a typical procedure, the precursor melamine was thermal treated in a tube furnace at 550 °C for 4 h with a heating rate of 2 °C min^{-1} under air atmosphere. The yellow-colored product was collected and ground into powder for further use. The G-g-C_3N_4 were prepared by thermal oxidation exfoliation of the pristine g-C_3N_4 obtained as above in static air as follows: 400 mg of the pristine g-C_3N_4 was placed in an open ceramic container and was heated at 500 °C for 2 h with a ramp rate of 5 °C min^{-1}. A light yellow powder of G-g-C_3N_4 was finally obtained with a yield of about 7.9%.

Synthesis of Ag/G-g-C_3N_4 nanocomposite

Fifty milligrams of as prepared G-g-C_3N_4 was dispersed in water (35 mL) by mild sonication for 5 min. One milligram $AgNO_3$ was added to this suspension and stirred in the dark for 1 h. With continuous nitrogen sparging, the resulting mixture was stirred under UV light for 1 h and washed thoroughly with distilled water and finally dried in a vacuum oven at 60 °C for further use.

Characterization

The phase purity of samples was analyzed by X-ray powder diffraction (XRD) using a Bruker D2 PHASER X-ray diffractometer with graphite monochromator using Cu Kα radiation (λ = 1.54184 Å) at room temperature. Fourier transform infrared spectra (FTIR) of the samples were recorded between 400 and 2000 cm^{-1} on a Nicolet NEXUS 670 FTIR spectrometer. Raman spectra were obtained using a Renishaw Raman system model 2000 spectrometer. X-ray photoelectron spectroscopy (XPS, PHI-5702, Physical Electronics) was performed using a monochromated Al Kα irradiation. The morphologies of different samples were observed by field emission scanning electron microscope (FESEM, Hitachi, S-4800), transmission electron microscopy (TEM) and high-resolution transmission electron microscopy (HRTEM, FEI Tecnai F30, operated at 300 kV). Diffuse reflectance ultraviolet-visible (UV-vis) absorption spectra were measured using a PerkinElmer 950 spectrometer, while $BaSO_4$ was used as a reference. The specific surface area of the samples was measured by the dynamic Brunauer–Emmett–Teller (BET) method, in which N_2 was adsorbed at 77 K using a Micromeritics ASAP 2000 system. Photoluminescence emission (PL) spectra were carried out by a FLS-920T spectrometer with Xe 900 (450 W xenon arc lamp) as the light source.

Evaluation of photocatalytic activity

The photocatalytic activity of the sample was evaluated by measuring the degradation ratio of methylene blue (MB). The initial concentration of MB solution was 10 mg L^{-1} and the used amount of photocatalyst was 0.1 g per 300 mL of MB solution. After the sample suspension was stirred for 40 min in the dark to realize the adsorption equilibrium, the photocatalytic reaction was started using a 350 W xenon lamp (with a cutoff filter of 420 nm) for the visible-light irradiation source. A series of a certain volume of suspension were withdrawn at selected times for analysis. After recovering the catalyst by centrifugation, the concentration of MB solution was analyzed by measuring the light absorption of the clear solution using a PerkinElmer 950 spectrometer. The light energy density is 40 mW cm^{-2} in the photocatalytic experiments.

Results and discussion

The crystal structure of as-prepared g-C_3N_4, G-g-C_3N_4 and Ag/G-g-C_3N_4 were analyzed by XRD patterns. As presented in Fig. 1, all of the peaks in the XRD patterns of the samples could be easily indexed to the hexagonal phase of g-C_3N_4 (JCPDS 87-1526). The peak at about 27° is due to the stacking of the conjugated aromatic system, which is indexed for graphitic materials as the (002) peak of g-C_3N_4. Another minor diffraction peak around 13° is assigned to the (100) plane associated with the in-plane repeated unites of g-C_3N_4.[21] With respect to the pristine g-C_3N_4, the peaks originated from the periodic stacking of layers in the G-g-C_3N_4 and Ag/G-g-C_3N_4 are shifted from 27.3° to 27.7°, indicating a decreased gallery distance between the basic sheets in the G-g-C_3N_4 and Ag/G-g-C_3N_4. The reason is that the single layer in bulk g-C_3N_4 is potentially undulated, but it could be planarized by further heating, resulting in a denser stacking.[23] No significant diffraction peaks of any other phases or

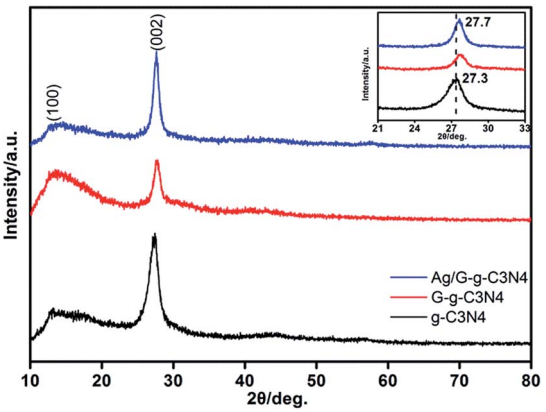

Fig. 1 XRD patterns of g-C_3N_4, G-g-C_3N_4 and Ag/G-g-C_3N_4.

impurities can be detected in the composite sample, which indicate that the introducing of Ag species does not affect the crystal structure of g-C_3N_4. What is more, no diffraction peaks of Ag species are detected, which may be explained by the small amounts of Ag species introducing (2 wt%) and high dispersion in the Ag/G-g-C_3N_4.

The crystal structure of the g-C_3N_4, G-g-C_3N_4 and Ag/G-g-C_3N_4 can be further confirmed by FTIR spectroscopy. As shown in Fig. 2, for pristine g-C_3N_4 sample, the broad peak at the range of 3000–3500 cm^{-1} corresponds to N–H stretching vibration of uncondensed amino groups and O–H vibration from adsorbed water on the surface.[24] The peak at 1638 cm^{-1} could be ascribed to C–N stretching and the four peaks at 1575 cm^{-1}, 1410 cm^{-1}, 1325 cm^{-1} and 1246 cm^{-1} can attribute to aromatic C–N stretching vibration.[25] The absorption peak at 807 cm^{-1} accords with characteristic breathing mode of triazine units.[26] All main characteristic vibration FTIR peaks related to g-C_3N_4 can be distinctly found in G-g-C_3N_4 and Ag/G-g-C_3N_4, suggesting that the overall structure of g-C_3N_4 keeps intact after thermal oxidation exfoliation and depositing the Ag nanoparticles, which is in accordance with XRD results.

Raman spectroscopy is usually used to search the vibrational properties of carbon materials. Fig. 3 shows Raman spectra of g-C_3N_4, G-g-C_3N_4 and Ag/G-g-C_3N_4 samples. There are no significant Raman signals observed on pristine g-C_3N_4 and G-g-C_3N_4, but a clear Raman spectrum is detected on Ag/G-g-C_3N_4. The band at 1569 cm^{-1} corresponds to C=N stretching vibration of g-C_3N_4, which is also defined as graphitic G band, indicating the formation of graphite like structure, while the 552 cm^{-1} belongs to in-plane symmetrical stretching vibration of heptazine heterocycles.[27] The peaks located at 475 cm^{-1}, and 1235 cm^{-1} stem from the vibration modes of CN heterocycles in g-C_3N_4.[28] In general, Raman intensity can be greatly enhanced by the electromagnetic interaction or coupling Ag nanoparticles with proper shape and size. Ling *et al.* reported that graphite-like materials also have the potential enhancing the Raman effects and found that the Raman enhancement factors can be distinguished through three classes that correspond to the symmetry of vibrations of the molecule.[29] Therefore, the enhancement of Raman intensity could be attributed to the

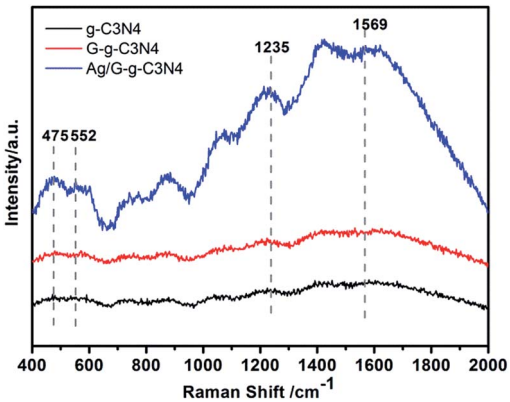

Fig. 3 Raman spectra of g-C_3N_4, G-g-C_3N_4 and Ag/G-g-C_3N_4.

charge transfer between Ag and the g-C_3N_4 molecules, originating from the plasma and Raman enhancement effects of Ag nanoparticles and g-C_3N_4 molecules,[30] respectively. The results convincingly demonstrate that an interaction exists between Ag and g-C_3N_4 molecules to facilitate charge transfer.

XPS was carried out to determine the chemical composition of the Ag/G-g-C_3N_4 sample and the valence states of various species present therein. Fig. 4a presents the survey spectrum of Ag/G-g-C_3N_4. The results indicated the presence of C, N, Ag and a small amount of O, which may be due to the surface absorption and oxidation. The C1s (Fig. 4b) spectrum of Ag/G-g-C_3N_4 could be fitted to four peaks at 284.6, 285.1, 288.0, and 288.5 eV, corresponding to the sp^2 C–C bonds, C–NH_2 species, N=C–N coordination and the N–C–O groups, respectively.[31] In addition, the sample exhibited N1s in Fig. 4c profiles with core levels at around 398.5, 399.1, and 401.1 eV, which could be attributed to sp^2-hybridized nitrogen (C–N=C), sp^3-hybridized nitrogen (N–C_3), and amino functional groups with a hydrogen atom (C–NH_2), respectively.[32] Fig. 4d shows the characteristic Ag3d peak that has a 6.0 eV splitting of the 3d doublet, which is corresponding to the metallic Ag^0 species.[21] This result confirms the presence of metallic Ag in the Ag/G-g-C_3N_4.

The morphology and micro structure of prepared samples were investigated with SEM and TEM as shown in Fig. 5.

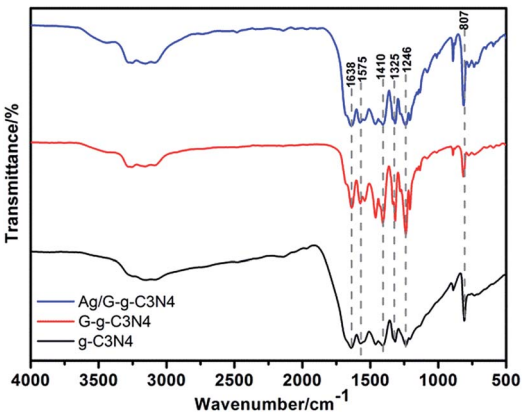

Fig. 2 FTIR spectra of g-C_3N_4, G-g-C_3N_4 and Ag/G-g-C_3N_4.

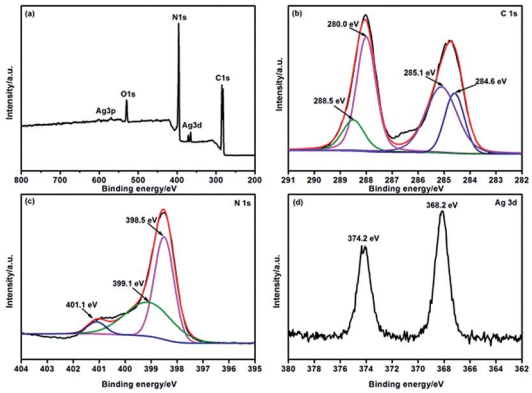

Fig. 4 XPS survey spectrum (a), high-resolution C1s spectrum (b), N1s spectrum (c) and Ag3d spectrum (d) of Ag/G-g-C_3N_4.

Compared to pristine g-C_3N_4 consisting of solid agglomerates with a size of several micrometers (Fig. 5a), the representative G-g-C_3N_4 appears as loose and soft agglomerates with a size of tens of micrometers (Fig. 5b). After photodeposition of Ag nanoparticles, Ag/G-g-C_3N_4 keeps the morphology of G-g-C_3N_4, and exhibits an exfoliated and wrinkled nanosheets texture characteristic (Fig. 5c). The high-magnification SEM image in Fig. 5d also confirms that the appearance of Ag/G-g-C_3N_4 is quite similar to that of graphene and Ag nanoparticles well dispersed on nanosheets. From the TEM image of Ag/G-g-C_3N_4 (Fig. 5e and f), Ag nanoparticles (black colored dots) with sizes about 10 nm can be found clearly, which are uniformly dispersed on the surface of the thin G-g-C_3N_4 nanosheets. Furthermore, we can observe that a very close connection existed between Ag and g-C_3N_4 to form the heterostructure, guaranteeing the charge transfer in the space smoothly. The inset in Fig. 5f is the HRTEM image of Ag/G-g-C_3N_4, which indicates that the lattice spacing is 0.236 nm, corresponding to the (111) lattice planes of metal Ag.[25]

The nitrogen adsorption–desorption isotherms in Fig. 6 show type IV isotherms with distinct H3 hysteresis loops, which use to calculated the BET specific surface areas. The BET specific surface areas of g-C_3N_4, and Ag/G-g-C_3N_4 are 5.55 and 189.9 $m^2\ g^{-1}$, respectively. The BET specific surface area was 34 times higher than that of pristine g-C_3N_4, which could provide abundant reactive sites and short bulk diffusion length for reducing the recombination probability of photoexcited charge carriers.[20]

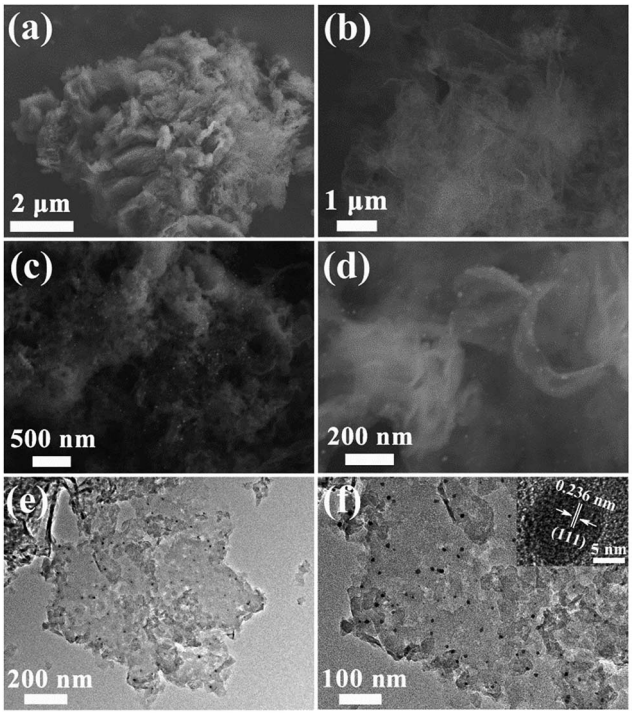

Fig. 5 SEM images of pristine g-C_3N_4 (a) and G-g-C_3N_4 (b). Low-(c) and high-magnification (d) SEM images of Ag/G-g-C_3N_4. Low-(e) and high magnification (e) TEM images of Ag/G-g-C_3N_4.

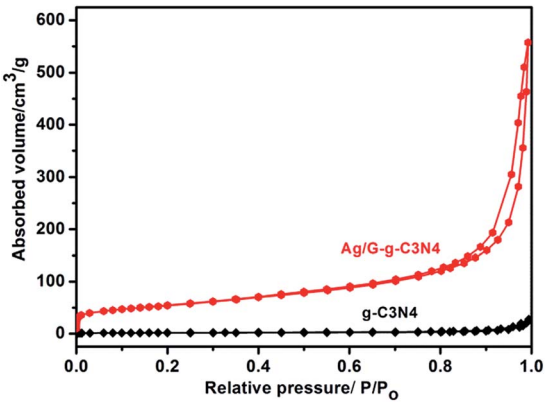

Fig. 6 N_2 adsorption–desorption isotherms of g-C_3N_4, and Ag/G-g-C_3N_4.

Optical absorption of the as-prepared g-C_3N_4, G-g-C_3N_4 and Ag/G-g-C_3N_4 were investigated using an UV-vis spectrometer. As shown in Fig. 7, an obvious blue shift of the intrinsic absorption edge in the G-g-C_3N_4 was observed with respect to the pristine g-C_3N_4. The derived band gaps are 2.95 and 2.54 eV for the G-g-C_3N_4 and the pristine g-C_3N_4. The reason for this larger bandgap is attributed to the well-known quantum confinement effect by shifting the conduction and valence band edges in opposite directions.[33] The larger bandgap of resultant G-g-C_3N_4 hinders its visible light absorption. However, compared with G-g-C_3N_4, when G-g-C_3N_4 coupled Ag nanoparticles, the absorption intensity in the visible light region is significantly improved, and the absorption edge red shift about 20 nm (0.14 eV), while the powder colors shift from white to grey with Ag loading. This phenomenon could be attributed to the surface plasmon resonance effect of Ag nanoparticles.[34]

To investigate the photocatalytic activity of the prepared samples, MB was chosen as are presentative hazardous dye to evaluate the photocatalytic performance, which showed a major absorption band at 664 nm. A blank test (without any photocatalyst) exhibited almost no self-degradation of MB. As show in Fig. 8a–c, the absorbance of MB decreases with increase of light

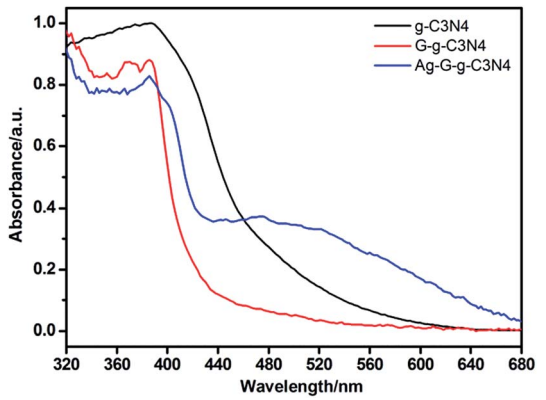

Fig. 7 UV-visible absorption spectra of g-C_3N_4, G-g-C_3N_4 and Ag/G-g-C_3N_4.

irradiation time, which indicates that all prepared samples have the photocatalytic degradation ability. Compared with g-C_3N_4 and G-g-C_3N_4, the Ag/G-g-C_3N_4 exhibits higher photocatalytic activity, which could completely degrade MB dye in 60 min under visible light irradiation. As shown in Fig. 8c, no absorbance peak is observed after visible light irradiation of 60 min, which indirectly proves that the MB molecules are destroyed or decomposed into small molecules completely. The degradation of dyes can be ascribed to a pseudo-first order reaction with a Langmuir–Hinshelwood model when C_0 is small: $\ln(C_0/C) = k_a t$, where k_a is the apparent first-order rate constant.[35] By calculated correspondingly degradation dynamics curves (Fig. 8d), the apparent rate constants (k_a, min^{-1}) are 0.004 min^{-1} for pristine g-C_3N_4 and 0.04 min^{-1} for Ag/G-g-C_3N_4 nanocomposite. It is clearly shows that Ag/G-g-C_3N_4 displayed an enhanced photocatalytic activity for MB degradation and the degradation rate was 10 times higher than that of pristine g-C_3N_4 under visible light irradiation. The enhancement of photocatalytic activity could be attributed to the surface plasmon resonance effect of Ag and large surface area of G-g-C_3N_4. TOC during the photocatalytic reactions was monitored to investigate the mineralization of MB. After visible light irradiation for 60 min (Fig. S1†), about 85% of total organic carbon (TOC) are removed, indicating that MB has not only been decolorized but also efficiently mineralized under visible light irradiation for Ag–G-g-C_3N_4.

From the viewpoint of pratical applications, the photocatalytic stability of the sample was evaluated by measuring the degradation ratio of MB in the same condition. As shown in Fig. 9a, the as-prepared Ag–G-g-C_3N_4 composite shows a good catalytic stability, maintaining a similar level of reactivity after four cycles. The slight decrease should originate from the inescapable loss of catalyst during the recycling process. The composition of the recyclable composite was also characterized by XPS. Fig. 9b shows the characteristic Ag3d peak that has a 6.0 eV splitting of the 3d doublet, which is corresponding to the metallic Ag^0 species. This result confirms that metallic Ag is stable after four cycles.

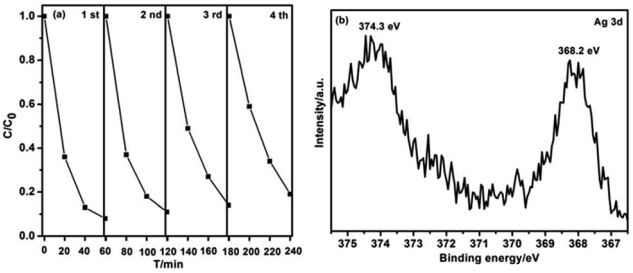

Fig. 9 (a) Circling runs in the presence of the Ag–G-g-C_3N_4 composite for photodegradation of MB dye under visible light; (b) high-resolution XPS spectra of Ag3d for Ag–G-g-C_3N_4 composite after the fourth cycle experiments irradiation.

Photoluminescence analysis is useful in revealing the efficiency of carrier transfer and separation, and investigating the lifetime of charge carriers. Fig. 10 shows the spectra of g-C_3N_4, G-g-C_3N_4 and Ag/G-g-C_3N_4 excited by 365 nm. From Fig. 9, it can be observed that there is a significant decrease in the PL intensity of Ag/G-g-C_3N_4 composite in comparison with that of the pristine g-C_3N_4. A weaker intensity of the peak means a lower recombination probability of photogenerated charge carriers.[17] Ag nanoparticles dispersed on the surface of G-g-C_3N_4, combined with the intimate interface between the two components, could effectively inhibit the recombination of photoinduced carriers, which is helpful for the separation of photogenerated electron–hole pairs in g-C_3N_4. Meanwhile, the Ag/G-g-C_3N_4 with enhanced visible light absorption should absorb more solar energy, the improved photogenerated carriers separation efficiency indicates that more charge carriers could be used by Ag/G-g-C_3N_4 composites. Therefore, the Ag/G-g-C_3N_4 photocatalyst possesses high photocatalytic performance. Fig. S2† show ESR spectra measured as the effect of light irradiation on the Ag–G-g-C_3N_4 composite. Just the signal of DMPO–$\cdot O_2^-$ are clearly observed when Ag–G-g-C_3N_4 composite are irradiated under light irradiation. Therefore, $\cdot O_2^-$ radicals are the main active species which play important roles during the photo-degradation process. These are also confirmed in the photodegradation of phenol (Fig. S3†).

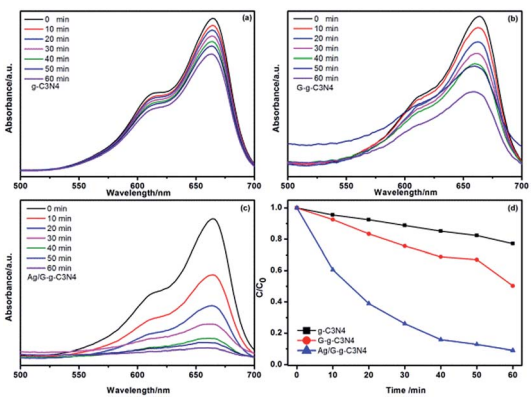

Fig. 8 Time-dependent absorption spectra of MB solution degraded by g-C_3N_4 (a), G-g-C_3N_4 (b) and Ag/G-g-C_3N_4 (c) under visible light irradiation. Correspondingly degradation dynamics curves of MB over above samples under visible light irradiation (d).

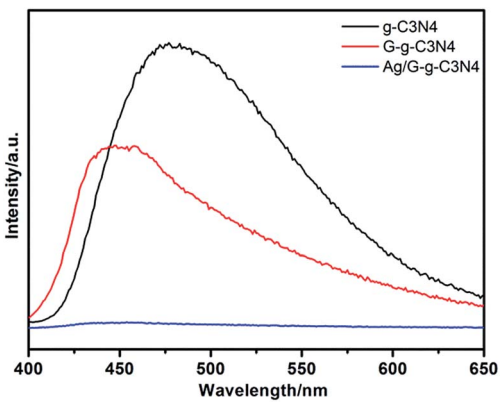

Fig. 10 PL spectra of g-C_3N_4, G-g-C_3N_4 and Ag/G-g-C_3N_4.

Conclusions

In summary, Ag/G-g-C_3N_4 photocatalyst was successfully synthesized by a simple thermal oxidation exfoliation-photo deposition technique. The monodispersed Ag nanoparticles were well dispersed on the surface of G-g-C_3N_4. The obtained Ag/G-g-C_3N_4 shows an enhanced photocatalytic activity than that of G-g-C_3N_4 and pristine g-C_3N_4 under visible light irradiation. Ag/G-g-C_3N_4 photocatalyst has the improved visible light absorption ability, abundant reactive sites as well as promoted photogenerated electron–hole pairs separation ability, which were derive from the synergic effect between the surface plasmon resonance effect of Ag nanoparticles and large surface area of G-g-C_3N_4. This work provides a promising approach to develop visible-light-response photocatalyst applied to pollutants degradation.

Acknowledgements

This research was supported by the International Sci. & Tech. Cooperation Foundation of Gansu Provincial, China (Grant No. 1504WKCA088 and 1304WCGA177) and the Fundamental Research Funds for the Central Universities (No. lzujbky-2016-131).

Notes and references

1 K. Li, Z. Zeng, L. Yan, S. Luo, X. Luo, M. Huo and Y. Guo, *Appl. Catal., B*, 2015, **165**, 428–437.
2 Q. Li, N. Zhang, Y. Yang, G. Wang and D. H. Ng, *Langmuir*, 2014, **30**, 8965–8972.
3 M. Tahir, C. Cao, F. K. Butt, S. Butt, F. Idrees, Z. Ali, I. Aslam, M. Tanveer, A. Mahmood and N. Mahmood, *CrystEngComm*, 2014, **16**, 1825.
4 Z. Zhu, Z. Lu, D. Wang, X. Tang, Y. Yan, W. Shi, Y. Wang, N. Gao, X. Yao and H. Dong, *Appl. Catal., B*, 2016, **182**, 115–122.
5 B. Liu, Y. Huang, Y. Wen, L. Du, W. Zeng, Y. Shi, F. Zhang, G. Zhu, X. Xu and Y. Wang, *J. Mater. Chem.*, 2012, **22**, 7484.
6 C. Han, Z. Chen, N. Zhang, J. C. Colmenares and Y.-J. Xu, *Adv. Funct. Mater.*, 2015, **25**, 221–229.
7 P. Dong, Y. Wang, B. Cao, S. Xin, L. Guo, J. Zhang and F. Li, *Appl. Catal., B*, 2013, **132–133**, 45–53.
8 J. Chen, S. Shen, P. Guo, M. Wang, J. Su, D. Zhao and L. Guo, *J. Mater. Res.*, 2013, **29**, 64–70.
9 X. Wang, K. Maeda, A. Thomas, K. Takanabe, G. Xin, J. M. Carlsson, K. Domen and M. Antonietti, *Nat. Mater.*, 2009, **8**, 76–80.
10 S. Samanta, S. Martha and K. Parida, *ChemCatChem*, 2014, **6**, 1453–1462.
11 J. Zhang, G. Zhang, X. Chen, S. Lin, L. Mohlmann, G. Dolega, G. Lipner, M. Antonietti, S. Blechert and X. Wang, *Angew. Chem., Int. Ed. Engl.*, 2012, **51**, 3183–3187.
12 X. Bai, S. Yan, J. Wang, L. Wang, W. Jiang, S. Wu, C. Sun and Y. Zhu, *J. Mater. Chem. A*, 2014, **2**, 17521–17529.
13 X. Wang, S. Wang, W. Hu, J. Cai, L. Zhang, L. Dong, L. Zhao and Y. He, *Mater. Lett.*, 2014, **115**, 53–56.
14 Y. Wang, J. Zhang, X. Wang, M. Antonietti and H. Li, *Angew. Chem., Int. Ed. Engl.*, 2010, **49**, 3356–3359.
15 P. Niu, G. Liu and H.-M. Cheng, *J. Phys. Chem. C*, 2012, **116**, 11013–11018.
16 S. C. Yan, S. B. Lv, Z. S. Li and Z. G. Zou, *Dalton Trans.*, 2010, **39**, 1488–1491.
17 J. Xue, S. Ma, Y. Zhou, Z. Zhang and M. He, *ACS Appl. Mater. Interfaces*, 2015, **7**, 9630–9637.
18 Y. Sun, T. Xiong, Z. Ni, J. Liu, F. Dong, W. Zhang and W.-K. Ho, *Appl. Surf. Sci.*, 2015, **358**, 356–362.
19 J. Sun, J. Zhang, M. Zhang, M. Antonietti, X. Fu and X. Wang, *Nat. Commun.*, 2012, 1139.
20 P. Niu, L. Zhang, G. Liu and H.-M. Cheng, *Adv. Funct. Mater.*, 2012, **22**, 4763–4770.
21 L. Ge, C. Han, J. Liu and Y. Li, *Appl. Catal., A*, 2011, **409–410**, 215–222.
22 Y. Bu, Z. Chen and W. Li, *Appl. Catal., B*, 2014, **144**, 622–630.
23 M. Groenewolt and M. Antonietti, *Adv. Mater.*, 2005, **17**, 1789–1792.
24 Z. Chen, P. Sun, B. Fan, Q. Liu, Z. Zhang and X. Fang, *Appl. Catal., B*, 2015, **170–171**, 10–16.
25 J. Qin, J. Huo, P. Zhang, J. Zeng, T. Wang and H. Zeng, *Nanoscale*, 2016, **8**, 2249–2259.
26 W. Bing, Z. Chen, H. Sun, P. Shi, N. Gao, J. Ren and X. Qu, *Nano Res.*, 2015, **8**, 1648–1658.
27 J. Jiang, L. Zhu, J. Zou, L. Ou-yang, A. Zheng and H. Tang, *Carbon*, 2015, **87**, 193–205.
28 J. Jiang, L. Ou-yang, L. Zhu, A. Zheng, J. Zou, X. Yi and H. Tang, *Carbon*, 2014, **80**, 213–221.
29 X. Ling, L. Xie, Y. Fang, H. Xu, H. Zhang, J. Kong, M. S. Dresselhaus, J. Zhang and Z. Liu, *Nano Lett.*, 2010, **10**, 553–561.
30 X. Bai, R. Zong, C. Li, D. Liu, Y. Liu and Y. Zhu, *Appl. Catal., B*, 2014, **147**, 82–91.
31 B. Long, J. Lin and X. Wang, *J. Mater. Chem. A*, 2014, **2**, 2942.
32 J. Li, B. Shen, Z. Hong, B. Lin, B. Gao and Y. Chen, *Chem. Commun.*, 2012, **48**, 12017–12019.
33 A. P. Alivisatos, *Science*, 1996, **271**, 933.
34 F. Fina, H. Menard and J. T. Irvine, *Phys. Chem. Chem. Phys.*, 2015, **17**, 13929–13936.
35 P. Dong, B. Liu, Y. Wang, H. Pei and S. Yin, *J. Mater. Res.*, 2011, **25**, 2392–2400.